Ain Shams Engineering Journal 12 (2021) 4099–4110

Contents lists available at ScienceDirect

Ain Shams Engineering Journal

journal homepage: www.sciencedirect.com

Engineering Physics and Mathematics

Non-coaxial rotation flow of MHD Casson nanofluid carbon nanotubes past a moving disk with porosity effect

Wan Nura'in Nabilah Noranuar [a], Ahmad Qushairi Mohamad [a,*], Sharidan Shafie [a], Ilyas Khan [b], Lim Yeou Jiann [a], Mohd Rijal Ilias [c]

[a] Department of Mathematical Sciences, Faculty of Science, Universiti Teknologi Malaysia, 81310 Johor Bahru, Johor, Malaysia
[b] Faculty of Mathematics and Statistics, Ton Duc Thang University, Ho Chi Minh City 72915, Viet Nam
[c] Centre of Mathematics Studies, Faculty of Computer and Mathematical Sciences, Universiti Teknologi MARA (UiTM), 40450 Shah Alam, Selangor, Malaysia

ARTICLE INFO

Article history:
Received 22 December 2020
Revised 22 February 2021
Accepted 2 March 2021
Available online 10 May 2021

Keywords:
Casson fluid
Carbon nanotubes
Laplace transform technique
Heat transfer
Moving disk

ABSTRACT

In this article, the fluid flow and heat transfer on MHD Casson nanofluid influenced by the non-coaxial rotation of moving disk passing through a porous medium is analyzed. A mixture of single-wall and multi-wall carbon nanotubes in the human Casson blood is used as the nanoparticles. Make use of the Laplace transform technique, the analytical solutions of the temperature and velocity profiles are obtained. The results show that the temperature and velocity profiles increase with the incorporation of CNTs. The nanofluid velocity reduces with a higher magnetic strength, but it is improved with the porosity. The imposition of CNTs has descended both primary and secondary skin friction and amplified the Nusselt number. SWCNTs have provided a greater heat transfer rate and skin friction as compared to MWCNTs. The obtained solution is verified when the present results show an excellent agreement with the published results and numerical values by Gaver-Stehfest algorithm.

1. Introduction

The non-Newtonian fluid is known as the fluid that disobeys Newton's Law of viscosity. Its applications have been widely encountered in diverse areas of industries such as food processing industries, bio-engineering processing, extraction of petroleum product from crude oil, drilling operations, and metallurgy process [1]. This fluid has a highly complex characteristic compared to the Newtonian fluid. Therefore, the industries demand a good simulation of this fluid flow, which is crucial to analyze their heat transfer system. Motivated by these factors, the complexity of non-Newtonian flow and its rheology have attracted scientists and researchers to expand their interest subjected to this field. The flow regimes of non-Newtonian fluid models with various geometries were found in Hussanan *et al.* [2], Saqib *et al.* [3] and Abdulhameed *et al.* [4]. The non-Newtonian fluids can be existed in different models due to different rheology such as Jeffrey, Maxwell, second grade, Brinkman type, power law, Bingham, Oldroyd-B, and Walter-B models [5]. One of the great discoveries on this type of fluid is Casson fluid. This type of fluid was firstly pioneered by Casson [6] to discuss the rheology of the pigment oil suspension flow of printing ink. This fluid behaves as viscoplastic, mainly influenced by the yield stress, which needs to be surpassed by the applied stress to induce fluid flow [7]. More precisely, the viscoplastic fluid tends to exhibit both elastic and solid behaviors that significantly depend on the applied stress [8]. The fluid experiences a likely solid phase when the yield stress is dominant and an elastic behaviour is exhibited when the flow is dominated by the applied stress [9]. Recently, the Casson model has been used to describe the characterictics of human blood [10]. Mukhopadhyay *et al.* [11] studied the non-Newtonian flow features of Casson fluid with an unsteady stretching sheet and was enlarged by Pramanik [12], imposing the exponentially radiative stretching sheet together with a porosity effect. Khalid *et al.* [13,14] investigated the Casson fluid flow behavior induced by free convection with an oscillating vertical plate and further expanded by Khalid *et al.* [15], introduc-

* Corresponding author.
E-mail addresses: wannurainnabilah189@gmail.com (W.N.N. Noranuar), ahmadqushairi@utm.my (A.Q. Mohamad), sharidan@utm.my (S. Shafie), ilyaskhanqau@yahoo.com (I. Khan), jiann8807@gmail.com (L.Y. Jiann), mrijal@uitm.edu.my (M.R. Ilias).
Peer review under responsibility of Ain Shams University.

Production and hosting by Elsevier

https://doi.org/10.1016/j.asej.2021.03.011
2090-4479/

ing the magnetic field and porosity effects in their study. They used Laplace transform technique to solve the momentum and energy equations with an oscillating boundary condition. The same approach was utilized by Khan *et al.* [16] to solve natural convection of MHD Casson fluid immersed in a porous medium past a moving vertical plate. This study suggested that the increase of Casson parameter and magnetic field decreased fluid velocity, while the increase of porosity increased fluid velocity. Ezzat [17] analyzed the MHD and porosity effects on free convection flow bounded with a porous vertical plate and they adopted a similar approach as in [15,16] to solve the problem. Ezzat [18] and Ezzat and Abd-Elaal [19] extended the work done by [17] by considering the flow of viscoelastic conducting fluid. All studies [17–19] revealed that porosity was the key factor in the enhancement of velocity but the magnetic field acted as the velocity retarded agent. Ezzat and Abd-Elaal [20] and Ezzat [21] improved the previous studies [17–19] by imposing the effect of a relaxation time on the flow. More relevant Casson fluid studies with several effects are available in Reddy *et al.* [22] and Das *et al.* [23].

The growing demand among emergence industries has recently made heat energy transfer a significant process in industrial applications. As a result, the heat transfer system with advanced features becomes a necessary to ensure the efficiency of the heating and cooling process. The implementation of nanotechnology in the heat transfer system can create a great opportunity for the industries to improve their energy performance, which may contribute to energy saving, reducing time processing, increasing thermal rate, and lengthen the working life equipment [24]. The indispensable factor in developing nanofluids as one of the strategies to enhance the heat transfer capabilities due to their high thermal conductivity has attracted numerous researchers' interest. The discussion on nanofluids was initiated by Choi and Eastman [25]. Nanofluid is a smartly engineered fluid that can enhance the fluid thermal conductivity by immersing the nanometer-sized particles into the convectional base fluid such as water, ethylene glycol, and mineral oils. The insertion of nanoparticles into base fluid results in the fluid's superior physical, mechanical, and electrical properties [26–29]. Recently, one such development in nanoparticles is carbon nanotubes (CNTs). They are found to have a unique property of aspect ratio, mechanical strength, electrical and mechanical conductivity, which provides them as the ideal candidates for industrial applications such as industrial cooling, fuel cells, nuclear reactors, sensing and imaging, microscale fluidic application, nanofluid coolant, drug delivery and cooling of microchips [30,31]. Anwar *et al.* [32] studied the porosity impact on the natural convective flow of nanofluid generated by moving vertical plate. The radiation and magnetic field effects were included, and the exact solution was obtained by applying the Laplace transform technique. Alwawi *et al.* [33] examined the influences of magnetic fields and surface heat flux from a solid sphere on the Casson nanofluid problem. CNTs in nanofluid are usually found in two types which are single-wall carbon nanotubes (SWCNTs) with a diameter of less than 1 nm and multi-wall carbon nanotubes (MWCNTs) made of several concentrically interlinked nanotubes with diameter more than 100 nm [34,35]. Khalid *et al.* [36] investigated the CNTs suspension impacts in Newtonian fluid flow by free convection phenomena without porosity and magnetic field effects. Khalid *et al.* [37] have included the impacts of magnetic field and porosity to study the heat transfer and flow of Casson fluid with CNTs suspension. In both studies, a vertical plate with an oscillating motion was considered, and the governing equations were solved by the Laplace transform technique. The investigation on natural convection flow with CNTs effect was presented by Saqib *et al.* [38] by considering flow past two parallel plates. Besides, Saqib *et al.* [39] reported the flow over a vertical microchannel. Saqib *et al.* [38,39] have chosen carboxy-methylcellulose (CMC) as the base fluid. Alkasasbheh *et al.* [40] investigated the heat transfer on Casson nanofluid MHD flow using both water and human blood as the base fluid to suspend CNTs particles over a stretching sheet.

The rotating fluid models are found in many situations encountered by engineering, especially in designing products such as jet engines, pumps, and vacuum cleaners. Since the rotating fluid gives a strong effect on the fluid motion from non-rotating fluid, this subject has fascinated many researchers' attention. The flow features and heat transfer with the rotating system in a circular pipe concentrating on the MHD effect were studied by Recebli *et al.* [41,42]. Their findings revealed that the velocity declined with the imposition of the magnetic field. The similar MHD impacts on the velocity profiles were also highlighted by Selimli *et al.* [43] and Selimli and Recebli [44] in the steady state of MHD liquid metal duct flow. Acharya *et al.* [45] carried out a comparative study of SWCNTs and MWCNTs in a rotating regime past a stretching sheet together with a magnetic field effect. They observed that the improvement of SWCNTs and MWCNTs volume fraction increased the nanofluid temperature. Besides, rotating nanofluid with SWCNTs has a higher temperature compared to MWCNTs. The other study on nanofluid CNTs flow in a rotating frame was also performed by Kumam *et al.* [46] and Shah *et al.* [47] . Meanwhile, Hayat *et al.* [48] investigated the non-Newtonian fluid at infinity in a porous medium with a non-coaxial rotation type. Then, it was expanded by Asghar *et al.* [49], considering an accelerated porous disk. Ersoy [50] continued the work by including suction and blowing cases. The slip condition and Hall current effects in a non-coaxial rotation of viscous fluid in a porous medium were analyzed by Guria *et al.* [51]. The results of the study show that the boundary layer thickness and velocity decreased with increasing magnetic and suction parameters. Next, the study of oscillating non-coaxial rotation disk in viscous fluid flow was presented by Ghara *et al.* [52], and they have considered the magnetic field and porosity effect in their study. A similar problem of an oscillating disk without the magnetic and porosity effects in the non-coaxial rotating viscous fluid was investigated by Mohamad *et al.* [53], and they applied the Laplace transform technique in solving their exact temperature and velocity solutions. Ersoy [54] extended the previous work by considering a disk executing non-torsional oscillation with the fluid having non-coaxial rotation at infinity. Mohamad *et al.* [55] examined the combined heat and mass transfer effects on the non-coaxial rotating flow and after that was furthered by Mohamad *et al.* [56], in taking magnetic and porosity effects into account. The disk executing cosine and sine oscillations was considered in both studies. Recently, Mohamad *et al.* [57] conducted a similar heat and mass transfer MHD problem in the non-coaxial rotation of oscillating porous disk but replacing the viscous fluid with second-grade fluid. Mohamad *et al.* [58] obtained the exact solutions for an accelerated non-coaxial rotation of MHD viscous fluid immersed in a porous medium. To the best of the authors' knowledge, the study on free convection flow of carbon nanotubes immersed in Casson nanofluid with non-coaxial rotation has not been emphasized in the literature or anywhere. Therefore, the present work aims to investigate the heat transfer and nanofluid flow of MHD Casson human blood with carbon nanotubes in a porous medium due to non-coaxial rotation by taking magnetic field and porosity into account. Exact solutions to the governing momentum and energy equations are obtained by implementing Laplace transform technique. The impacts of pertinent parameters on temperature and velocity profiles are graphically illustrated, coupled with a comprehensive discussion.

2. Mathematical model

Consider the non-coaxial rotation of an incompressible Casson nanofluid is unsteadily flowed by free convection with a moving vertical disk. The upward direction is referred to the x-axis of the disk while normal to the plane of disk is referred to the z-axis. The space $z > 0$ is occupied with the Casson nanofluid of constant kinematic viscosity υ_{nf} and it was bounded by a moving disk at $z = 0$. The medium in this study is considered to be porous and is filled with the Casson nanofluid, which is made up by the mixture of CNTs (SWCNTs or MWCNTs) and human blood. Both disk and nanofluid have rotated, and their axes are considered to be in plane $x = 0$. When $t = 0$, both nanofluid and disk initially rotate on z'-axis with a consistent angular velocity Ω and temperature T_∞. Later, when $t > 0$, the disk starts to move and rotate on z-axis, while the nanofluid at infinity remains to rotate on z'-axis. Both rotations have a consistent angular velocity Ω with the temperature of the disk raises to T_w. The two axes of rotation are separated by a distance, known as ℓ. A uniform strength of the transverse magnetic field B_0 is applied along the normal to the disk passing through the porous medium. The geometry illustrating the problem is shown in Fig. 1. The rheological equation which describes the relation of shear stress and strain rate for the incompressible flow of a Casson fluid can be written as follows [2,13,15,37]

$$\tau_{ij} = \begin{cases} 2\left(\mu + \frac{p_y}{\sqrt{2\pi}}\right)e_{ij}, \pi > \pi_c \\ 2\left(\mu + \frac{p_y}{\sqrt{2\pi_c}}\right)e_{ij}, \pi < \pi_c \end{cases}$$

where $\pi = e_{ij}e_{ij}$ and e_{ij} is the $(i,j)^{th}$ component of deformation rate, π is the product of the component of deformation rate with itself,π_c is a critical value of this product based on the non-Newtonian model, μ is the plastic dynamic viscosity of the non-Newtonian fluid and p_y is the yield stress of fluid. Under the above stated assumptions along with the Boussinesq approximation and the nanofluid model proposed by Tiwari and Das [59], the problem is governed by the momentum and energy equations as

$$\rho_{nf}\frac{\partial F}{\partial t} + dF = \mu_{nf}\left(1 + \frac{1}{\gamma}\right)\frac{\partial^2 F}{\partial z^2} + d\ell + (\rho\beta_T)_{nf}g_x(T - T_\infty) \tag{1}$$

$$(\rho C_p)_{nf}\frac{\partial T}{\partial t} = k_{nf}\frac{\partial^2 T}{\partial z^2} \tag{2}$$

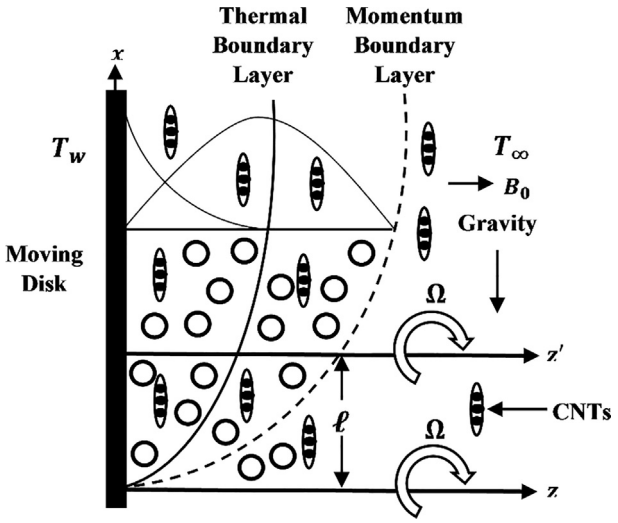

Fig. 1. Geometry of the problem.

with associated initial and boundary conditions as

$$F(z,0) = \Omega\ell, T(z,0) = T_\infty; z > 0$$

$$F(0,t) = U_0, T(0,t) = T_w; t > 0$$

$$F(\infty,t) = \Omega\ell, T(\infty,t) = T_\infty; t > 0 \tag{3}$$

where $d = \rho_{nf}\Omega i + \sigma_{nf}{B_0}^2 + \mu_{nf}/k_1$. The velocity for a rotating fluid is introduced in the form of complex velocity $F = F(z,t) = f(z,t) + ig(z,t)$ where $f(z,t)$ is (real part) primary velocity and $g(z,t)$ is (imaginary part) secondary velocities. Besides, $T = T(z,t)$ is the nanofluid temperature, $\gamma = \mu\sqrt{2\pi_c}/p_y$ is Casson parameter, k_1 is the permeability of porous medium, g_x is the acceleration due to gravity, and $U_0$is characteristic of velocity. The thermophysical properties in Casson nanofluid with CNTs involves thermal conductivity k_{nf}, electric conductivity σ_{nf}, dynamic viscosity μ_{nf}, density ρ_{nf}, heat capacitance $(\rho C_p)_{nf}$, and thermal expansion coefficient for temperature $(\rho\beta_T)_{nf}$ where all are clearly defined as in (4).

The nanofluid thermal conductivity and dimensionless heat transfer rate in this study are analyzed by applying the theoretical model introduced by Xue [60]. This model is established based on Maxwell theory by taking into account the rotating elliptical nanotubes with a substantial axial ratio and offsetting the space distribution impacts on CNTs. Thus, the model is given as

$$\mu_{nf} = \frac{\mu_f}{(1-\phi)^{2.5}}, \beta_{nf} = \frac{(1-\phi)(\rho\beta)_{nf} + \phi(\rho\beta)_{CNTs}}{\rho_{nf}},$$

$$\rho_{nf} = (1-\phi)\rho_{nf} + \phi\rho_{CNTs},$$

$$(\rho C_p)_{nf} = (1-\phi)(\rho C_p)_{nf} + \phi(\rho C_p)_{CNTs},$$

$$\frac{\sigma_{nf}}{\sigma_f} = \left\{1 + \frac{3\left(\frac{\sigma_{CNTs}}{\sigma_f} - 1\right)\phi}{\left(\frac{\sigma_{CNTs}}{\sigma_f} + 2\right) - \phi\left(\frac{\sigma_{CNTs}}{\sigma_f} - 1\right)}\right\},$$

$$\frac{k_{nf}}{k_f} = \frac{1 - \phi + 2\phi\frac{k_{CNTs}}{k_{CNTs}-k_f}ln\frac{k_{CNTs}+k_f}{2k_f}}{1 - \phi + 2\phi\frac{k_f}{k_{CNTs}-k_f}ln\frac{k_{CNTs}+k_f}{2k_f}} \tag{4}$$

where the subscripts $CNTs$ and f denote to carbon nanotubes and fluid, and ϕ is the nanofluid solid volume fraction, which afterwards are used based on their particular thermophysical properties as tabulated in Table 1.

The appropriate non-dimensional variables are introduced as

$$F^* = \frac{F}{\Omega\ell} - 1, z^* = \sqrt{\frac{\Omega}{\upsilon}}z, t^* = \Omega t, T^* = \frac{T - T_\infty}{T_w - T_\infty} \tag{5}$$

After employing the variables in Eq. (5) and the nanofluid model in Eq. (4) on the system of equations, Eqs. (1), (2) and (3) reduce to

$$\frac{\partial F}{\partial t} + d_1 F = \frac{1}{\phi_1}\left(1 + \frac{1}{\gamma}\right)\frac{\partial^2 F}{\partial z^2} + \phi_3 GrT \tag{6}$$

$$\frac{\partial T}{\partial t} = \frac{1}{a_1}\frac{\partial^2 T}{\partial z^2} \tag{7}$$

and their non-dimensional conditions become

$$F(z,0) = 0, T(z,0) = 0; z > 0$$

$$F(0,t) = U - 1, T(0,t) = 1; t > 0$$

$$F(\infty,t) = 0, T(\infty,t) = 0; t > 0 \tag{8}$$

where

Table 1
Thermophysical properties of Casson fluid, SWCNTs and MWCNTs.

Properties Material	$\rho\ (Kgm^{-3})$	$C_p\ \left(JKg^{-1}K^{-1}\right)$	$k\ \left(Wm^{-1}K^{-1}\right)$	$\sigma\ (Sm^{-1})$	$\beta \times 10^{-5}\ \left(K^{-1}\right)$
Human blood	1053	3594	0.492	0.8	0.18
SWCNTs	2600	425	6600	27×10^{-5}	$10^6 - 10^7$
MWCNTs	1600	796	3000	44×10^{-5}	1.9×10^{-4}

$$d_1 = \left(\mathrm{i} + M^2\phi_2 + \frac{1}{\phi_1 K}\right), a_1 = \frac{Pr\phi_4}{\lambda}, \lambda = \frac{k_{nf}}{k_f}, \phi_4 = (1-\phi) + \frac{\phi(\rho C_p)_{CNTs}}{(\rho C_p)_f},$$

$$\phi_1 = (1-\phi)^{2.5}\left((1-\phi) + \frac{\phi\rho_{CNTs}}{\rho_f}\right), \phi_3 = \frac{(1-\phi) + \frac{\phi(\rho\beta)_{CNTs}}{(\rho\beta)_f}}{(1-\phi) + \frac{\phi\rho_{CNTs}}{\rho_f}},$$

$$\phi_2 = \left(1 + \frac{3\left(\frac{\sigma_{CNTs}}{\sigma_f} - 1\right)\phi}{\left(\frac{\sigma_{CNTs}}{\sigma_f} + 2\right) - \phi\left(\frac{\sigma_{CNTs}}{\sigma_f} - 1\right)}\right)\frac{1}{\left((1-\phi) + \frac{\phi\rho_{CNTs}}{\rho_f}\right)}$$

are the constant parameters. The dimensionless parameters such as Prandtl number Pr, Grashof number Gr, magnetic M, porosity K parameters, and amplitude of disk U are defined as

$$Pr = \frac{\upsilon_f(\rho C_p)_f}{k_f}, Gr = \frac{g_x\beta_{Tf}(T_w - T_\infty)}{\Omega^2\ell}, M = \frac{\sigma_f {B_0}^2}{\Omega\rho_f}, \frac{1}{K} = \frac{\upsilon_f}{k_1\Omega}, U = \frac{U_0}{\Omega\ell}.$$

3. Exact solutions

Making use of the Laplace transform technique, the system of governing equations (6), (7), and (8) are converted from partial differential equations (PDEs) into a set of ordinary differential equations (ODEs) system. Thus, we have

$$\frac{d^2}{dz^2}\bar{F}(z,q) - (n_1 q + n_2)\bar{F}(z,q) = -n_3 Gr\,\bar{T}(z,q) \tag{9}$$

$$\frac{d^2}{dz^2}\bar{T}(z,q) - (a_1 q)\bar{T}(z,q) = 0 \tag{10}$$

$$\bar{F}(0,q) = (U-1)\frac{1}{q}, \bar{F}(\infty,q) = 0 \tag{11}$$

$$\bar{T}(0,q) = \frac{1}{q}, \bar{T}(\infty,q) = 0 \tag{12}$$

Then, the boundary conditions in Eq. (11) and Eq. (12) are used to solve Eq. (9) and Eq. (10). The solutions are

$$\bar{F}(z,q) = \frac{U}{q}exp(-z\sqrt{n_1}\sqrt{q+n_7}) - \frac{1}{q}exp(-z\sqrt{n_1}\sqrt{q+n_7}) - \frac{n_6 Gr}{q}exp(-z\sqrt{n_1}\sqrt{q+n_7}) + \frac{n_6 Gr}{q-n_5}exp(-z\sqrt{n_1}\sqrt{q+n_7}) + \frac{n_6 Gr}{q}exp(-z\sqrt{a_1 q}) - \frac{n_6 Gr}{q-n_5}exp(-z\sqrt{a_1 q}) \tag{13}$$

$$\bar{T}(z,q) = \frac{1}{q}exp(-z\sqrt{a_1 q}) \tag{14}$$

Employing inverse Laplace transform on Eq. (13) and Eq. (14), the exact solutions for velocity and temperature profiles form as

$$F(z,t) = F_1(z,t) - F_2(z,t) - F_3(z,t) + F_4(z,t) + F_5(z,t) - F_6(z,t) \tag{15}$$

$$T(z,t) = erfc\left(\frac{z}{2}\sqrt{\frac{a_1}{t}}\right) \tag{16}$$

with

$$F_1(z,t) = \frac{U}{2}\left[exp(z\sqrt{n_1 n_7})erfc\left(\frac{z}{2}\sqrt{\frac{n_1}{t}} + \sqrt{n_7 t}\right) + exp(-z\sqrt{n_1 n_7})erfc\left(\frac{z}{2}\sqrt{\frac{n_1}{t}} - \sqrt{n_7 t}\right)\right],$$

$$F_2(z,t) = \frac{1}{2}\left[exp(z\sqrt{n_1 n_7})erfc\left(\frac{z}{2}\sqrt{\frac{n_1}{t}} + \sqrt{n_7 t}\right) + exp(-z\sqrt{n_1 n_7})\left(\frac{z}{2}\sqrt{\frac{n_1}{t}} - \sqrt{n_7 t}\right)\right],$$

$$F_3(z,t) = \frac{n_6 Gr}{2}\left[exp(z\sqrt{n_1 n_7})erfc\left(\frac{z}{2}\sqrt{\frac{n_1}{t}} + \sqrt{n_7 t}\right) + exp(-z\sqrt{n_1 n_7})erfc\left(\frac{z}{2}\sqrt{\frac{n_1}{t}} - \sqrt{n_7 t}\right)\right],$$

$$F_4(z,t) = \frac{n_6 Gr}{2}\left[exp(n_5 t + z\sqrt{n_1(n_5+n_7)})erfc\left(\frac{z}{2}\sqrt{\frac{n_1}{t}} + \sqrt{(n_5+n_7)t}\right) + exp(n_5 t - z\sqrt{n_1(n_5+n_7)})erfc\left(\frac{z}{2}\sqrt{\frac{n_1}{t}} - \sqrt{(n_5+n_7)t}\right)\right],$$

$$F_5(z,t) = n_6 Gr\left[erfc\left(\frac{z}{2}\sqrt{\frac{a_1}{t}}\right)\right],$$

$$F_6(z,t) = \frac{n_6 Gr}{2}\left[exp(n_5 t + z\sqrt{a_1 n_5})erfc\left(\frac{z}{2}\sqrt{\frac{a_1}{t}} + \sqrt{n_5 t}\right) + exp(n_5 t - z\sqrt{a_1 n_5})erfc\left(\frac{z}{2}\sqrt{\frac{a_1}{t}} - \sqrt{n_5 t}\right)\right],$$

where

$$n_0 = \frac{\gamma}{\gamma+1}, n_1 = \phi_1 n_0, n_2 = d_1 n_1, n_3 = \phi_3 n_1, n_4 = a_1 - n_1, n_5 = \frac{n_2}{n_4},$$

$$n_6 = \frac{n_3}{n_4 n_5}, n_7 = \frac{n_2}{n_1}.$$

4. Skin friction and Nusselt number

Skin friction is evaluated to determine the shear stress at the boundary, and its dimensional form of Casson nanofluid is given as [15,23]

$$\tau = -\mu_{nf}\left(1 + \frac{1}{\gamma}\right)\left.\frac{\partial F}{\partial z}\right|_{z=0} \tag{17}$$

After the dimensionless process, Eq. (17) reduces to

$$\tau = -\frac{1}{(1-\phi)^{2.5}}\left(1+\frac{1}{\gamma}\right)\left.\frac{\partial F}{\partial z}\right|_{z=0} \tag{18}$$

where $\tau^* = \tau\sqrt{v_f}/\Omega^{\frac{3}{2}}\ell\mu_f$. By substituting Eq. (15) into Eq. (18), the solution yields

$$\tau(t) = \tau_1(t) - \tau_2(t) - \tau_3(t) + \tau_4(t) + \tau_5(t) - \tau_6(t) \tag{19}$$

where

$$\tau_1(t) = U\left[\sqrt{n_1 n_7}erfc\left(\sqrt{n_7 t}\right) - \sqrt{n_1 n_7} - \frac{\sqrt{n_1}exp(-n_7 t)}{\sqrt{\pi t}}\right],$$

$$\tau_2(t) = \sqrt{n_1 n_7}erfc\left(\sqrt{n_7 t}\right) - \sqrt{n_1 n_7} - \frac{\sqrt{n_1}exp(-n_7 t)}{\sqrt{\pi t}},$$

$$\tau_3(t) = n_6 Gr\left[\sqrt{n_1 n_7}erfc\left(\sqrt{n_7 t}\right) - \sqrt{n_1 n_7} - \frac{\sqrt{n_1}exp(-n_7 t)}{\sqrt{\pi t}}\right],$$

$$\tau_4(t) = n_6 Gr\left[\sqrt{n_1(n_5+n_7)}exp(n_5 t)erfc\left(\sqrt{(n_5+n_7)t}\right) - \sqrt{n_1(n_5+n_7)}exp(n_5 t) - \frac{\sqrt{n_1}exp(-n_7 t)}{\sqrt{\pi t}}\right],$$

$$\tau_5(t) = -n_6 Gr\left[\sqrt{\frac{a_1}{\pi t}}\right],$$

$$\tau_6(t) = n_6 Gr\left[\sqrt{a_1 n_5}exp(n_5 t)erfc\left(\sqrt{n_5 t}\right) - \sqrt{a_1 n_5}exp(n_5 t) - \sqrt{\frac{a_1}{\pi t}}\right].$$

Nusselt number is evaluated to analyze the heat transfer rate and describes the convective ratio to conductive heat transfer. The Nusselt number is presented as [38]

$$Nu = -\frac{k_{nf}}{k_f}\left.\frac{\partial T}{\partial z}\right|_{z=0} = \lambda\sqrt{\frac{a_1}{\pi t}}. \tag{20}$$

5. Results and discussion

In this paper, the heat transfer problem on non-coaxial rotating MHD Casson nanofluid flow passed through a porous medium with a moving disk is solved using Laplace transform method. The human blood base fluid is used to suspend both CNTs nanoparticles (SWCNTs and MWCNTs). At this part, with the help of pictorial illustration, the influences of Grashof number Gr, Casson parameter γ, magnetic field parameter M, porosity parameter K, nanoparticle volume fraction ϕ, dimensionless time t, and amplitude of disk U on the physical behaviour of velocity and temperature profiles are further analyzed. Since the rotating nanofluid regime is involved in this problem, the graphs for velocity profile are presented in primary f and secondary g velocities, which respectively are defined by the real part and the imaginary part of velocity. From these graphs, the obtained solutions satisfy both initial and boundary conditions. Furthermore, the numerical results for skin friction and Nusselt number Nu are also presented in Table 2 and Table 3 with τ_p and τ_s are denoted for primary skin friction and secondary skin friction, respectively. To check the validity of the obtained solutions, the present results are compared to published results by Mohamad *et al.* [53]. The identical profile of Eq. (15) for both SWCNTs and MWCNTs in present results and Eq. (53) in published results are observed as in Fig. 11 by allowing parameter of nanoparticle volume fraction and magnetic field $\phi = M = 0$, porosity $K \to \infty$, and Casson parameter $\gamma \to \infty$ in the present results, and letting $\omega = 0$ in the published results. Further, the present velocity solution is also verified with the numerical Gaver-Stehfest algorithm [61,62] as tabulated in Table 4. This algorithm provides a numerical inversion of Laplace transform and its numerical values is used to compare with the exact solutions. The results from the comparison have satisfied with small error. Hence, the validity of the obtained solution is verified.

The effect of different values of time t on f and g profiles for both SWCNTs and MWCNTs in Casson nanofluid are depicted in Fig. 2. From these figures, the growth in both f and g profiles for the cases of SWCNTs and MWCNTs are reported when the values of t increase. This effect is possible because the buoyancy force is enhanced when time increases, and this creates the external sources that will continuously supply energy to the flow. When flow gets more energy, both velocity profiles of Casson nanofluid with SWCNTs and MWCNTs increase. Table 2 estimates SWCNTs and MWCNTs to have a drop in τ_p with a percentage of 35.78% and 35.72%, and a drop in τ_s with 37.27% and 37.21% decrement. A slight difference of rate which is less than 0.1% is observed between SWCNTs and MWCNTs but the highest rate is still given by SWCNTs. The same effect is also reported for the temperature profile in Fig. 3, where the increase in t results in the rising of Casson nanofluid temperature for both SWCNTs and MWCNTs. A similar impact of t on velocity and temperature profiles are found in [5,13,53,55,56]. The nanofluid has high temperature when the flow is near the surface due to applied wall temperature, and it gradually decreases when the nanofluid flow away from the surface.

Fig. 4 illustrates the Grashof number Gr impacts on f and g profiles for Casson nanofluid with SWCNTs and MWCNTs. The results

Table 2
Primary τ_p and secondary τ_s skin friction for SWCNTs and MWCNTs.

	Gr	K	M	γ	ϕ	U	SWCNTs		MWCNTs	
							τ_p	τ_s	τ_p	τ_s
0.2	**0.5**	**2**	**0.2**	**0.5**	**0.02**	**2**	2.0636	−0.4419	2.0464	−0.4375
0.4							1.3253	−0.6066	1.3155	−0.6003
0.6							0.9821	−0.7204	0.9758	−0.7126
	5						−2.1736	−0.4771	−2.1607	−0.4719
	10						−6.8815	−0.5163	−6.8352	−0.5100
		3					1.9881	−0.4468	1.9702	−0.4425
		5					1.9271	−0.4508	1.9087	−0.4465
			3				5.2543	−0.2767	5.0306	−0.2810
			5				8.8358	−0.1772	8.4386	−0.1816
				0.8			1.7335	−0.3836	1.7188	−0.3799
				1.0			1.6121	−0.3621	1.5983	−0.3585
					0.12		−0.7561	−0.5792	−0.8215	−0.5472
					0.22		−5.3366	−0.7837	−5.4572	−0.7111
						3	4.5980	−0.8799	4.5602	−0.8713
						4	7.1324	−1.3178	7.0740	−1.3050

Table 3
Nusselt number *Nu* for SWCNTs and MWCNTs.

t	ϕ	*Nu*		Enhancement / Decrement Rate	
		SWCNCTs	MWCNTs	SWCNTs	MWCNTs
0.2	**0.02**	6.6932	6.6165	–	–
0.4		4.7328	4.6785	−29.299%	−29.290%
0.6		3.8643	3.8200	−18.351%	−18.350%
	0.12	10.2010	9.9017	52.41%	49.65%
	0.22	12.9773	12.5550	27.22%	26.80%

Table 4
Comparison of present velocity result with Gaver-Stehfest algorithm at $t = 0.2$, $Gr = 0.5$, $K = 2$, $M = 0.2$, $\gamma = 0.5$, $\phi = 0.02$, $U = 2$ and $\Pr = 21$.

z	SWCNTs				MWCNTs			
	Present results		Gaver-Stehfest		Present results		Gaver-Stehfest	
	Primary	Secondary	Primary	Secondary	Primary	Secondary	Primary	Secondary
0	1.0000	0.0000	1.0000	0.0000	1.0000	0.0000	1.0000	0.0000
0.5	0.6371	0.0367	0.6371	0.0367	0.6398	0.0366	0.6398	0.0366
1.0	0.3484	0.0339	0.3484	0.0339	0.3524	0.0340	0.3524	0.0340
1.5	0.1636	0.0203	0.1636	0.0204	0.1672	0.0207	0.1672	0.0207
2.0	0.0651	0.0093	0.0652	0.0093	0.0675	0.0096	0.0675	0.0096
2.5	0.0218	0.0034	0.0219	0.0034	0.0230	0.0036	0.0230	0.0036
3.0	0.0061	0.0010	0.0061	0.0010	0.0066	0.0011	0.0066	0.0011
3.5	0.0014	0.0002	0.0014	0.0002	0.0016	0.0003	0.0015	0.0003
4.0	0.0003	0.0000	0.0003	0.0000	0.0003	0.0000	0.0003	0.0000

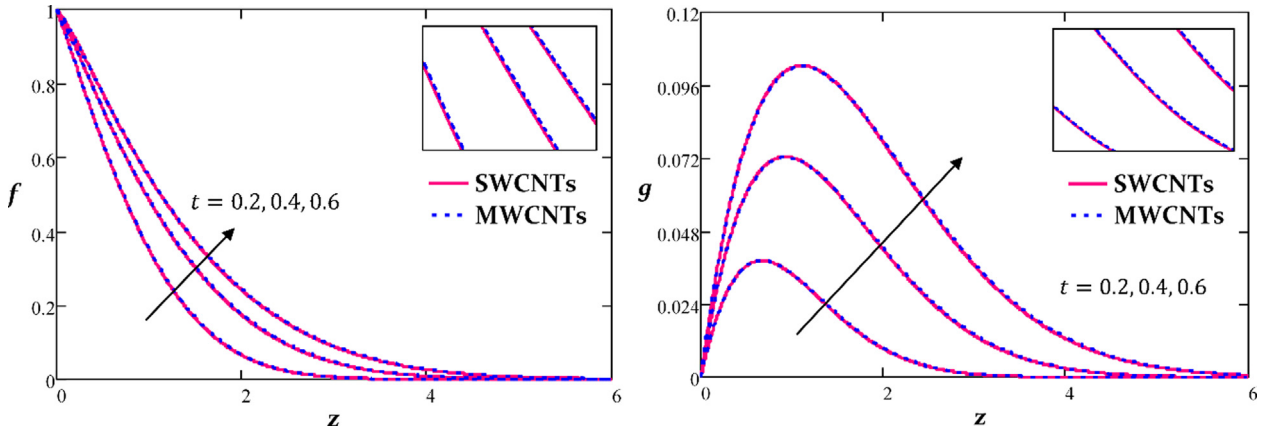

Fig. 2. Impact t on primary f and secondary g velocity profile with $\gamma = 0.5, \Pr = 21, Gr = 0.5, K = 2, M = 0.2, \phi = 0.02$and.$U = 2$

show that f and g profiles for SWCNTs and MWCNTs increase with increasing values of Gr. This behavior is induced by the domination of buoyancy forces created by an increase in the temperature gradient. Consequently, viscous force is diminished, and this leads to increase f and g profiles of Casson nanofluid. This velocity propagation under the influence of Gr has been also mentioned in [15,29,39]. In this figure, both types of CNTs have the same nature on velocity profiles. A clear illustration of their effects is presented in the zooming box as depicted in the figures. It suggests that both f and g profiles for MWCNTs are higher than SWCNTs. This is due to MWCNTs has a low density, which causes their velocity profiles to be prominent.

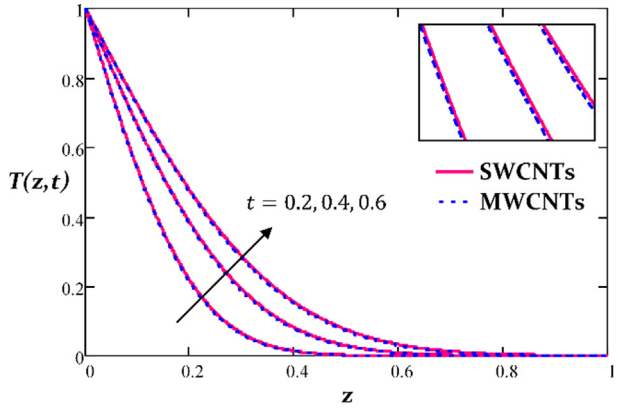

Fig. 3. Impact of t on temperature profile with $\Pr = 21$ and.$\phi = 0.02$

The identical behavior is noticed in both f and g profiles for Casson nanofluid with SWCNTs and MWCNTs under the impact of porosity parameter K as shown in Fig. 5. Both types of CNTs depict the increasing trend for both f and g profiles of Casson nanofluid with increasing K, which has also been observed by [29,32]. By having a high porous medium, the nanofluid able to flow passing through it at a high speed. This behavior is possible because when values of K increase, the applied pressure gradient in a medium and drag effect acting opposite to the flow decrease, and therefore, escalate both f and g profiles of Casson nanofluid with SWCNTs and MWCNTs. In this figure, the changes in f and g profiles have insignificantly seemed. However, by assisting with the zooming

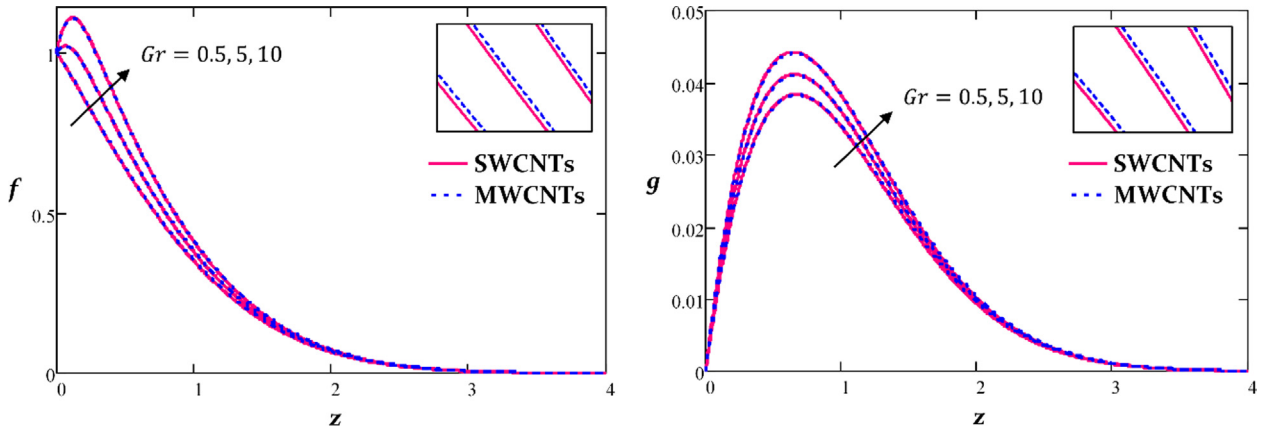

Fig. 4. Impact of Gr on primary f and secondary g profile with $\gamma = 0.5, \mathrm{Pr} = 21, K = 2, M = 0.2, \phi = 0.02, t = 0.2$ and $U = 2$

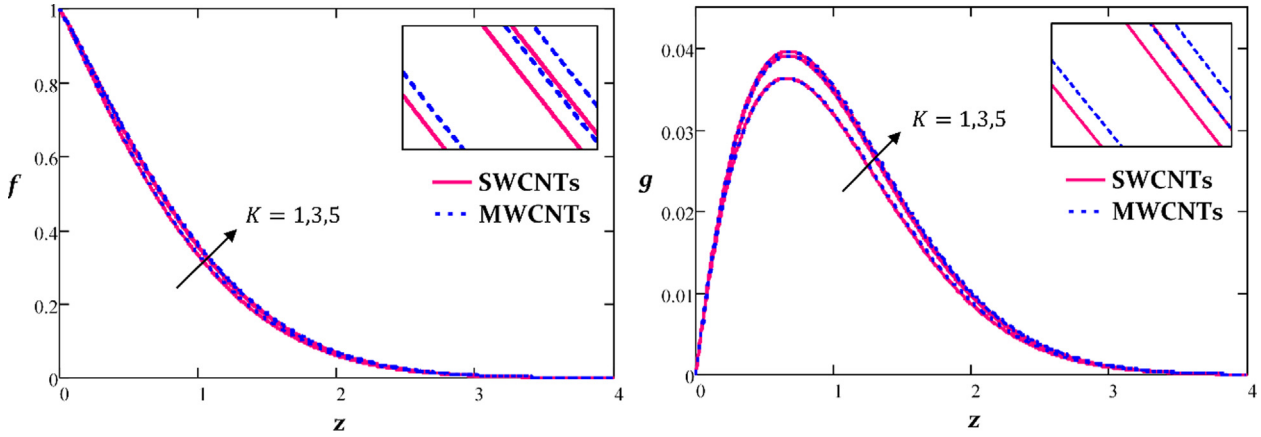

Fig. 5. Impact of K on primary f and secondary g profile with $\gamma = 0.5, \mathrm{Pr} = 21, Gr = 0.5, M = 0.2, \phi = 0.02, t = 0.2$ and $U = 2$

part, it is clearly observed that velocity of Casson nanofluid with MWCNTs is prominent compared to SWCNTs, and it reflects the same reason as discussed in Fig. 4. This effect is also supported by the low skin friction of MWCNTs in Table 2, which causes less friction drag on the surface. The diminution rate of τ_p and τ_s are 3.66% and 1.11% for SWCNTs and 3.72% and 1.14% for MWCNTs, which proves that SWCNTs have an inferior rate compared to MWCNTs.

Fig. 6 reports the reverse effects on both f and g profiles for Casson nanofluid with SWCNTs and MWCNTs in the presence of magnetic field M. Both profiles for SWCNTs and MWCNTs descend as M increases. The diminution of velocity is due to the conqueror of Lorentz forces, which is created by the presence of electric and magnetic fields. This forces have acted as the frictional forces and become the key factor in slowing down the nanofluid's velocity. Therefore, when M increases, the nanofluid experiences a high resistance, and the nanofluid flow is retarded, which is also followed by the decrease in momentum boundary layer thickness. This particular impact of M on velocity can be justified with [16,39,40]. Moreover, under this influence, Casson nanofluid with MWCNTs have a prominent effect on both f and g profiles than SWCNTs due to the same factor discussed in Figs. 4 and 5. It is quite clear from Table 2 that SWCNTs have high τ_p and τ_s than MWCNTs, which implies that the surface has experienced a great friction drag and affects their low velocity profiles. Its changing rate of τ_p and τ_s are also 9% and 1.61% less than of the changing rate by MWCNTs. Overall from Fig. 6 and Table 2, when compared to the other effects, it suggests that magnetic field has a major and significant impact on the velocity profiles. Thus, it may be useful in several applications, such as in the medical field, the blood flow in the body can be controlled by regulating the intensity of the applied magnetic field.

The impact of Casson parameter γ on the physical behavior of f and g for Casson nanofluid with SWCNTs and MWCNTs can be found in Fig. 7. It is useful to note that Casson fluid is known as viscoplastic fluid, where the non-Newtonian behavior is affected by the value of γ. As γ increases, the shear stress of fluid exceeds the yield stress, which causes the fluid to act like a Newtonian fluid and leads the flow to be faster. In the figure, the effect of increment γ value is followed by an amplification in fluid plasticity, which then reduces the momentum boundary layer thickness and f profile. [8,15,23,37] have reported the same statement for the velocity profile of Casson fluid. Such behavior is clearly noticed within the interval $0.5 \leq z \leq 2$ and then, f profile gradually approaches the boundary condition after $z \geq 2$. However, the g profile for both types of CNTs exhibit both increasing and decreasing trend, which has been greatly affected by the presence of yield stress. The g profile increases until it achieves the utmost velocity at $z = 0.5$ and afterward declines as it goes far from the surface. Furthermore, due to the low density of MWCNTs, it causes f and g profiles of Casson nanofluid with MWCNTs to be prominent and also seems to have a slow rate of velocity decrement compared to SWCNTs. Table 2 reveals that MWCNTs have less τ_p and high τ_s than SWCNTs. Moreover, the values of τ_p reduce and the values of τ_s increase for both CNTs in favour of γ. Comparatively, SWCNTs has exceeded 0.85% of τ_p and less 0.97% of τ_s from MWCNTs.

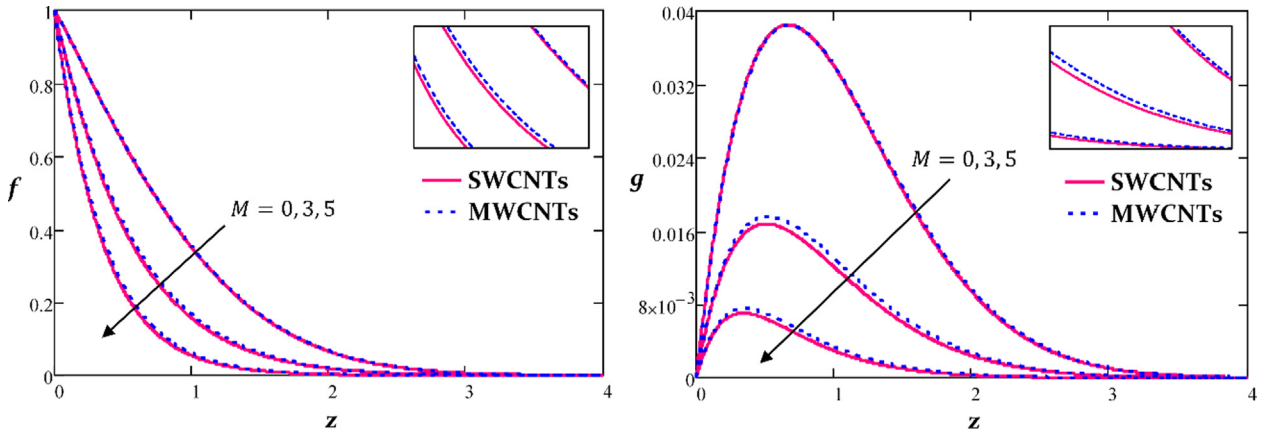

Fig. 6. Impact of M on primary f and secondary g profile with $\gamma = 0.5, \mathrm{Pr} = 21, Gr = 0.5, K = 2, \phi = 0.02, t = 0.2$ and $U = 2$

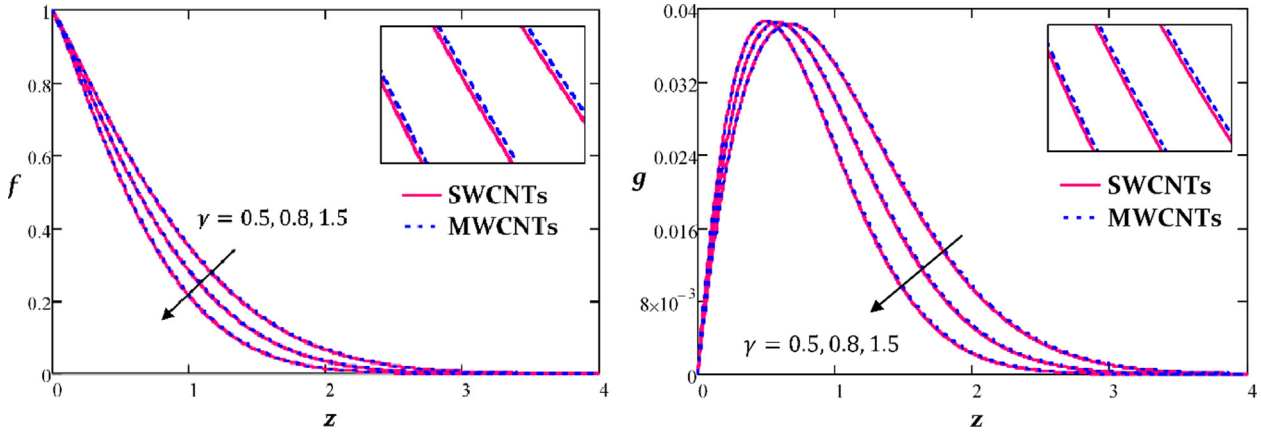

Fig. 7. Impact of γ on primary f and secondary g profile with $M = 0.2, \mathrm{Pr} = 21, Gr = 0.5, K = 2, \phi = 0.02, t = 0.2$ and $U = 2$

Fig. 8 justifies the effect of different nanoparticles volume fraction ϕ on f and g profiles for SWCNTs and MWCNTs cases. The figures reveal that f and g profiles of Casson nanofluid with SWCNTs and MWCNTs enhance with increasing values of ϕ. This nature of velocity propagation is clearly visualized within the interval $0 \leq z \leq 2.5$ for the f profile and $0.5 \leq z \leq 3$ for the g profiles. The enhancement in velocity profile when the carbon nanotubes are added to human blood may contribute to some of the health benefits, particularly in the development of drug delivery process, in order to help the drug transportation specifically to the cancerous growth as well as to the damaged arteries areas in the fight against cardiovascular disease. As discussed previously, MWCNTs confirms a high-velocity profile than SWCNTs due to their low density properties, which also assures it to have small values of τ_p as in Table 2. This effect causes MWCNTs to experience less friction drag at the surface and have a high velocity distribution. Both CNTs nanofluids have reported decreasing τ_p and increasing τ_p with ϕ. The effect of different values of ϕ on Casson nanofluid temperature for SWCNTs and MWCNTs is depicted in Fig. 9, where the increase in ϕ results in the growth of temperature profile for both types of CNTs. This is because the insertion of more CNTs in human blood enhances the nanofluid's thermal conductiv-

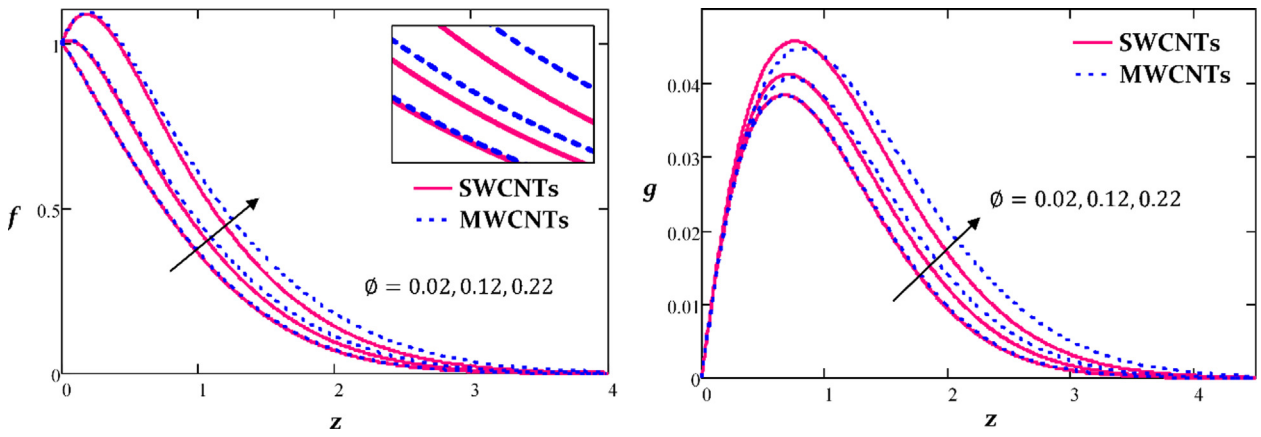

Fig. 8. Impact of ϕ on primary f and secondary g profile with $M = 0.2, \mathrm{Pr} = 21, Gr = 0.5, K = 2, \gamma = 0.5, t = 0.2$ and $U = 2$

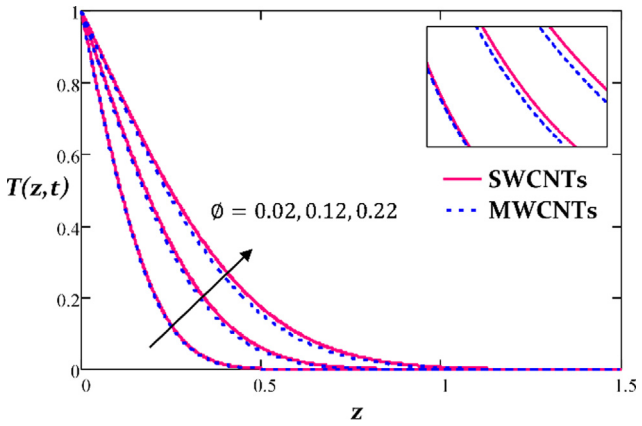

Fig. 9. Impact of ϕ on temperature profile with $t = 0.2$ and.Pr $= 21$

ity and directly improves the ability of nanofluid to conduct heat. This characteristic proves that the fluid with high volume of CNTs can conduct more heat, which results in the hike of temperature distribution and enlarges the thermal boundary layer. In Fig. 9, it is clearly observed that Casson nanofluid's temperature in the presence of SWCNTs is higher compared to MWCNTs. This effect is due to the high thermal conductivity of SWCNTs, which provides a better conduction of heat. Table 3 observes that *Nu* for SWCNTs and MWCNTs augment with the rate 52.41% and 49.65%, respectively correspond to the rising values of ϕ. This result directly implies to the reduction of nanofluid heat capacitance, which leads to increase the rate of heat transfer. The similar trend of velocity and temperature distributions can be found in [34,45].

After that, Fig. 10 discusses the influence of different disk amplitude U values on f and g profiles for Casson nanofluid with SWCNTs and MWCNTs. The results show that an increase in U increases both f and g profiles for Casson nanofluid with both types of CNTs and ascends the values of τ_p. This is because the external forces that moving disk has created, are used to rotate the fluid and amplify the friction between the fluid and disk. These forces help CNTs to give full reaction at all regions of rotating fluid. This results can be verified with the study of [32,53]. Under this influence, the velocity of Casson nanofluid in the presence of MWCNTs seems to be higher than SWCNTs due to the same reason as discusses for Figs. 4 to 8. MWCNTs also have high τ_p and less τ_s compared to SWCNTs. Overall for the impacts of CNTs on the velocity and temperature profiles, comparatively, SWCNTs have a low-velocity profile and a high-temperature profile compared to MWCNTs. These effects are significantly affected by its low density and high thermal conductivity properties, which has been highlighted in [30,34].

6. Conclusion

The current study on the unsteady free convection flow of MHD Casson nanofluid induced by non-coaxial rotations with a moving plate embedded in a porous medium is investigated, where it has been greatly inspired from the previous works [37,53]. A new mathematical model of Casson nanofluid with non-coaxial rotation is introduced. The effects of MHD and porosity are taken into account. The study of Casson nanofluid involves a mixture of

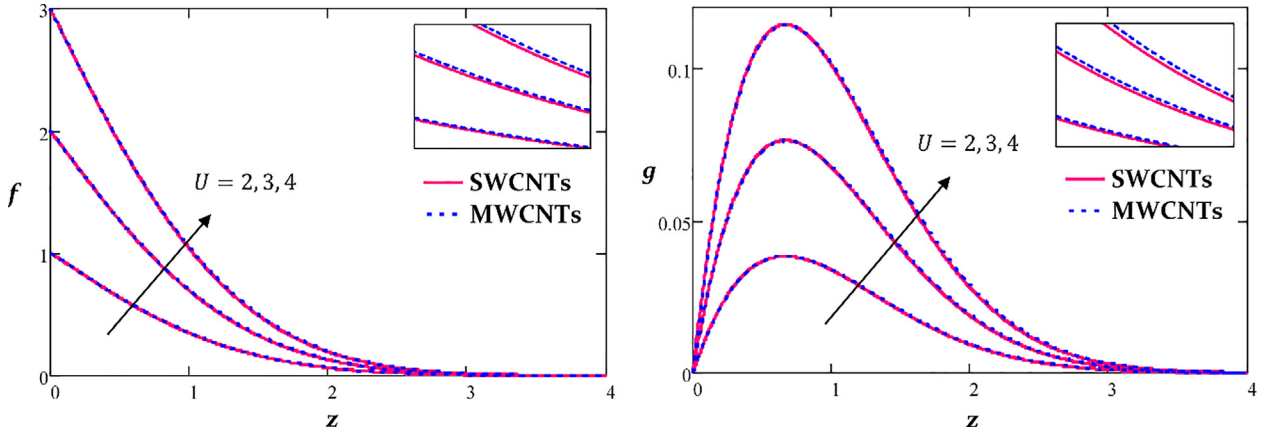

Fig. 10. . Impact of U on primary f and secondary g profile with $M = 0.2, \text{Pr} = 21, Gr = 0.5, K = 2, \gamma = 0.5, t = 0.2$ and.$\phi = 0.02$

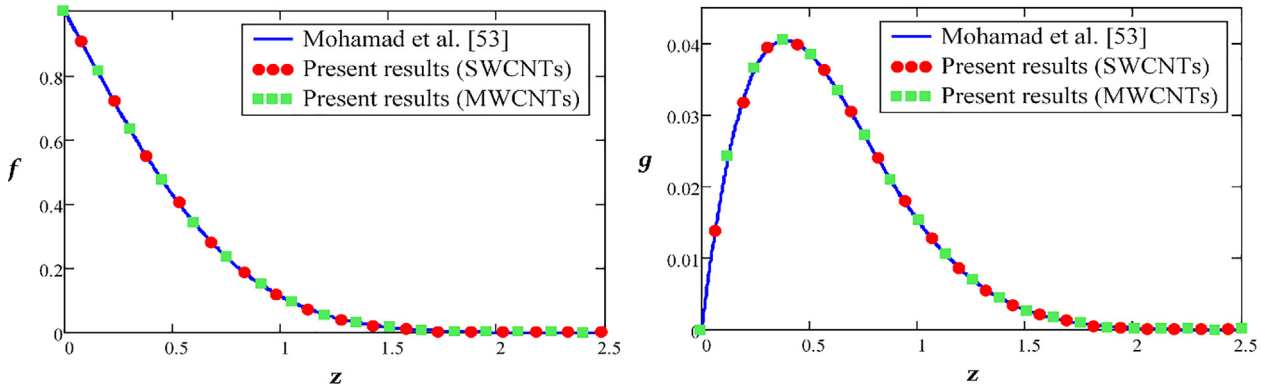

Fig. 11. . Comparison between published results by [53] and present results on primary and secondary velocity profile.

human blood suspending SWCNTs and MWCNTs. The exact temperature and velocity solutions are generated by using the Laplace transform method. The verification process is conducted by comparing the present results with published results from Mohamad *et al.* [53] and numerical values from Gaver-Stehfest algorithm. The validity of the obtained solution is confirmed when an excellent agreement is observed for both comparisons. The findings in this study mainly contribute to analyze and control the flow and heat transfer of rotating Casson nanofluid, where it can be implemented specifically in a rotating human blood system. The model can also be used in medical applications as the magnetic field's imposition is important to treat the cancerous or damaged cell. The significant results of this study are concluded as follows:

i. Both primary and secondary velocity profiles of Casson nanofluid for both SWCNTs and MWCNTs increase when Gr, K, t, ϕ and U increase.
ii. As M increases, both primary and secondary velocity profiles of Casson nanofluid for both SWCNTs and MWCNTs decrease while as γ increases, only the primary velocity profile decreases and secondary velocity profile shows a fluctuating trend.
iii. Increasing values of ϕ and t cause an increment in the temperature profile of Casson nanofluid for both SWCNTs and MWCNTs.
iv. For primary and secondary velocity profile, Casson nanofluid with MWCNTs is higher than Casson nanofluid with SWCNTs due to a low density of MWCNTs.
v. For temperature profile, Casson nanofluid with SWCNTs is higher than Casson nanofluid with MWCNTs due to SWCNTs' high thermal conductivity.
vi. An increase of $\phi, Gr, K,$ and t decreases both primary and secondary skin friction, while the increase of M increases both primary and secondary skin friction.
vii. The Nusselt number for both types CNTs nanofluids increase with increasing ϕ but decrease with increasing t.
viii. The rate of heat transfer is enhanced with the suspension of high values of ϕ. The amount of heat transfer and its increment rate by SWCNTs suspension is greater than MWCNTs suspension.

Declaration of Competing Interest

The authors declare that they have no known competing financial interests or personal relationships that could have appeared to influence the work reported in this paper.

Acknowledgement

The authors would like to acknowledge the Ministry of Higher Education Malaysia and Research Management Centre-UTM, Universiti Teknologi Malaysia (UTM) for financial support through vote numbers 17J98, FRGS/1/2019/STG06/UTM/02/22 and 08G33.

References

[1] Aneja M, Chandra A, Sharma S. Natural convection in a partially heated porous cavity to Casson fluid. Int Commun Heat Mass Transf 2020;114:. doi: https://doi.org/10.1016/j.icheatmasstransfer.2020.104555104555.
[2] Hussanan A, Anwar MI, Ali F, Khan I, Shafie S. Natural convection flow past an oscillating plate with Newtonian heating. Heat Transf Res 2014;45(2):119–35. doi: https://doi.org/10.1615/HeatTransRes.2013006385.
[3] Saqib M, Ali F, Khan I, Sheikh NA, Jan SAA. Samiulhaq Exact solutions for free convection flow of generalized Jeffrey fluid: A Caputo-Fabrizio fractional model. Alexandria Eng J 2018;57(3):1849–58. doi: https://doi.org/10.1016/j.aej.2017.03.017.
[4] Abdulhameed M, Khan I, Vieru D, Shafie S. Exact solutions for unsteady flow of second grade fluid generated by oscillating wall with transpiration. Appl Math Mech 2014;35(7):821–30. doi: https://doi.org/10.1007/s10483-014-1837-9.
[5] Hussanan A, Salleh MZ, Tahar RM, Khan I. Unsteady boundary layer flow and heat transfer of a Casson fluid past an oscillating vertical plate with Newtonian heating. PLoS ONE 2014;9(10):1–9. doi: https://doi.org/10.1371/journal.pone.0108763.
[6] Casson N. A flow equation for pigment-oil suspensions of the printing ink type. Rheology of Disperse Systems 1959:84–104.
[7] Chhabra RP, Richardson JF. Non-Newtonian flow and applied rheology: engineering applications. United State: Butterworth-Heinemann; 2011.
[8] Gbadeyan JA, Titiloye EO, Adeosun AT. Effect of variable thermal conductivity and viscosity on Casson nanofluid flow with convective heating and velocity slip. Heliyon 2020;6(1):1-10. doi: https://doi.org/10.1016/j.heliyon.2019.e03076
[9] Irgens F. Rheology and non-newtonian fluids. New York: Springer; 2014.
[10] Ali F, Sheikh NA, Khan I, Saqib M. Solutions with Wright Function for Time Fractional Free Convection Flow of Casson Fluid. Arab J Sci Eng 2017;42(6):2565–72. doi: https://doi.org/10.1007/s13369-017-2521-3.
[11] Mukhopadhyay S, De PR, Bhattacharyya K, Layek GC. Casson fluid flow over an unsteady stretching surface. Ain Shams Eng J 2013;4(4):933–8. doi: https://doi.org/10.1016/j.asej.2013.04.004.
[12] Pramanik S. Casson fluid flow and heat transfer past an exponentially porous stretching surface in presence of thermal radiation. Ain Shams Eng J 2014;5(1):205–12. doi: https://doi.org/10.1016/j.asej.2013.05.003.
[13] Khalid A, Khan I, Shafie S. Exact solutions for unsteady free convection flow of Casson fluid over an oscillating vertical plate with constant wall temperature. Abstract Appl Anal 2015;2015:1–8. doi: https://doi.org/10.1155/2015/946350.
[14] Khalid A, Khan I, Shafie S. Unsteady boundary layer flow of a Casson fluid past an oscillating vertical plate with constant wall temperature. Malaysian J Fundam Appl Sci 2015;11(1):1–5.
[15] Khalid A, Khan I, Khan A, Shafie S. Unsteady MHD free convection flow of Casson fluid past over an oscillating vertical plate embedded in a porous medium. Eng Sci Technol 2015;18(3):309–17. doi: https://doi.org/10.1016/j.jestch.2014.12.006.
[16] Khan D, Khan A, Khan I, Ali F, Ul Karim F, Tlili I. Effects of relative magnetic field, chemical reaction, heat generation and Newtonian heating on convection flow of Casson fluid over a moving vertical plate embedded in a porous medium. Sci Rep 2019;9(1):1–18. doi: https://doi.org/10.1038/s41598-018-36243-0.
[17] Ezzat MA. State space approach to unsteady two-dimensional free convection flow through a porous medium. Can J Phys 1994;72(5–6):311–7. doi: https://doi.org/10.1139/p94-045.
[18] Ezzat MA, Zakaria M, Shaker O, Barakat F. State space formulation to viscoelastic fluid flow of magnetohydrodynamic free convection through a porous medium. Acta Mech 1996;119:147–64. doi: https://doi.org/10.1139/p94-045.
[19] Ezzat MA, Abd-Elaal MZ. State space approach to viscoelastic fluid flow of hydromagnetic fluctuating boundary-layer through a porous medium. J Appl Math Mech 1997;77(3):197–207. doi: https://doi.org/10.1002/zamm.19970770307.
[20] Ezzat MA, Abd-Elaal MZ. Free convection effects on viscoelastic boundary layer flow with one relaxation time through a porous medium. J Franklin Inst 1997;334(4):685–706. doi: https://doi.org/10.1016/S0016-0032(96)00095-6.
[21] Ezzat MA. Free convection effects on perfectly conducting fluid. Int J Eng Sci 2001;39(7):799–819. doi: https://doi.org/10.1016/S0020-7225(00)00059-8.
[22] Reddy GJ, Raju RS, Rao JA. Influence of viscous dissipation on unsteady MHD natural convective flow of Casson fluid over an oscillating vertical plate via FEM. Ain Shams Eng J 2018;9(4):1907–15. doi: https://doi.org/10.1016/j.asej.2016.10.012.
[23] Das M, Mahato R, Nandkeolyar R. Newtonian heating effect on unsteady hydromagnetic Casson fluid flow past a flat plate with heat and mass transfer. Alexandria Eng J 2015;54(4):871–9. doi: https://doi.org/10.1016/j.aej.2015.07.007.
[24] Sivashanmugam P. Application of nanofluids in heat transfer. An overview of heat transfer phenomena 2012;16.
[25] Choi SU, Eastman JA. Enhancing thermal conductivity of fluids with nanoparticles. United States: Argonne National Lab; 1995.
[26] Khan MS, Karim I, Ali LE, Islam A. Unsteady MHD free convection boundary-layer flow of a nanofluid along a stretching sheet with thermal radiation and viscous dissipation effects. Int Nano Lett 2012;2(1):1–24. doi: https://doi.org/10.1186/2228-5326-2-24.
[27] Hamad MAA, Pop I, Md Ismail AI. Magnetic field effects on free convection flow of a nanofluid past a vertical semi-infinite flat plate. Nonlinear Anal Real World Appl 2011;12(3):1338–46. doi: https://doi.org/10.1016/j.nonrwa.2010.09.014.
[28] Das S, Jana RN. Natural convective magneto-nanofluid flow and radiative heat transfer past a moving vertical plate. Alexandria Eng J 2015;54(1):55–64. doi: https://doi.org/10.1016/j.aej.2015.01.001.
[29] Zin NAM, Khan I, Shafie S, Alshomrani AS. Analysis of heat transfer for unsteady MHD free convection flow of rotating Jeffrey nanofluid saturated in a porous medium. Results Phys 2017;7:288–309. doi: https://doi.org/10.1016/j.rinp.2016.12.032.
[30] Gul T, Akbar R, Zaheer Z, Amiri IS. The impact of the Marangoni convection and magnetic field versus blood-based carbon nanotube nanofluids. J Nanomater Nanoeng Nanosyst 2019;234(1–2):37–46. doi: https://doi.org/10.1177/2397791419872892.

[31] Khan ZH, Khan WA, Haq RU, Usman M, Hamid M. Effects of volume fraction on water-based carbon nanotubes flow in a right-angle trapezoidal cavity: FEM based analysis. Int Commun Heat Mass Transf 2020;116:. doi: https://doi.org/10.1016/j.icheatmasstransfer.2020.104640104640.
[32] Anwar T, Kumam P, Shah Z, Watthayu W, Thounthong P. Unsteady radiative natural convective MHD nanofluid flow past a porous moving vertical plate with heat source/sink. Molecules 2020;25(4):854. doi: https://doi.org/10.3390/molecules25040854.
[33] Alwawi FA, Alkasasbeh HT, Rashad AM, Idris R. Natural convection flow of sodium alginate based Casson nanofluid about a solid sphere in the presence of a magnetic field with constant surface heat flux. J Phys Conf Ser 2019;1366(1):. doi: https://doi.org/10.1088/1742-6596/1366/1/012005012005.
[34] Ebaid A, Al Sharif MA. Application of Laplace transform for the exact effect of a magnetic field on heat transfer of carbon nanotubes-suspended nanofluids. Zeitschrift für Naturforschung A. 2015;70(6):471–5. doi: https://doi.org/10.1515/zna-2015-0125.
[35] Aman S, Khan I, Ismail Z, Salleh MZ, Alshomrani AS, Alghamdi MS. Magnetic field effect on Poiseuille flow and heat transfer of carbon nanotubes along a vertical channel filled with Casson fluid. AIP Adv 2017;7(1):. doi: https://doi.org/10.1063/1.4975219015036.
[36] Khalid A, Jiann LY, Khan I, Shafie S. Exact solutions for unsteady free convection flow of carbon nanotubes over an oscillating vertical plate. AIP Conf Proc 2017;1830:0200054. doi: https://doi.org/10.1063/1.4980917.
[37] Khalid A, Khan I, Khan A, Shafie S, Tlili I. Case study of MHD blood flow in a porous medium with CNTS and thermal analysis. Case Stud Therm Eng 2018;12:374–80. doi: https://doi.org/10.1016/j.csite.2018.04.004.
[38] Saqib M, Khan I, Shafie S. Natural convection channel flow of CMC-based CNTs nanofluid. Eur Phys J Plus 2018;133(12):49.
[39] Saqib M, Khan I, Shafie S. Application of Atangana-Baleanu fractional derivative to MHD channel flow of CMC-based-CNT's nanofluid through a porous medium. Choas, Solitons Fractals 2018;116(1):79–85. doi: https://doi.org/10.1016/j.chaos.2018.09.007.
[40] Alkasasbheh HT, Swalmeh MZ, Saeed HGB, Al Faqih FM, Talafha AG. Investigation on CNTs-water and human blood based Casson nanofluid flow over a stretching sheet under impact of magnetic field. Front Heat Mass Transf 2020;14:1–7. doi: https://doi.org/10.5098/hmt.14.15.
[41] Recebli Z, Selimli S, Ozkaymak M. Theoretical analyses of immiscible MHD pipe flow. Int J Hydrog Energy 2015;40(44):15365–73. doi: https://doi.org/10.1016/j.ijhydene.2015.04.010.
[42] Recebli Z, Gedik E, Selimli S. Electrical field effect on three-dimensional magnetohydrodynamic pipe flow: a CFD study. Progr Comput Fluid Dynam Int J 2016;16(4):261–70. doi: https://doi.org/10.1504/PCFD.2016.077293.
[43] Selimli S, Recebli Z, Arcaklioglu E. MHD numerical analyses of hydrodynamically developing laminar liquid lithium duct flow. Int J Hydrog Energy 2015;40(44):15358–64. doi: https://doi.org/10.1016/j.ijhydene.2015.02.020.
[44] Selimli S, Recebli Z. Impact of electrical and magnetic field on cooling process of liquid metal duct magnetohydrodynamic flow. Therm Sci 2018;22 (1):263–71. doi: https://doi.org/10.2298/TSCI151110147S.
[45] Acharya N, Das K, Kundu PK. Rotating flow of carbon nanotube over a stretching surface in the presence of magnetic field: a comparative study. Appl Nanosci 2018;8(3):369–78. doi: https://doi.org/10.1007/s13204-018-0794-9.
[46] Kumam P, Shah Z, Dawar A, Rasheed HU, Islam S. Entropy generation in MHD radiative flow of CNTS Casson nanofluid in rotating channels with heat source/sink. Math Probl Eng 2019;2019:1–14. doi: https://doi.org/10.1155/2019/9158093.
[47] Shah Z, Bonyah E, Islam S, Gul T. Impact of thermal radiation on electrical MHD rotating flow of carbon nanotubes over a stretching sheet. AIP Adv 2019;9(1):. doi: https://doi.org/10.1063/1.5048078015115.
[48] Hayat T, Ellahi R, Asghar S, Siddiqui AM. Flow induced by non-coaxial rotation of a porous disk executing non-torsional oscillations and a second grade fluid rotating at infinity. Appl Math Model 2004;28(6):591–605. doi: https://doi.org/10.1016/j.apm.2003.10.011.
[49] Asghar S, Hanif K, Hayat T, Khalique CM. MHD non-Newtonian flow due to non-coaxial rotations of an accelerated disk and a fluid at infinity. Commun Nonlinear Sci Numer Simul 2007;12(4):465–85. doi: https://doi.org/10.1016/j.cnsns.2005.04.006.
[50] Ersoy HV. MHD flow of a second order/grade fluid due to noncoaxial rotation of a porous disk and the fluid at infinity. Math Comput Appl 2010;15 (3):354–63. doi: https://doi.org/10.3390/mca15030354.
[51] Guria M, Kanch AK, Das S, Jana RN. Effects of Hall current and slip condition on unsteady flow of a viscous fluid due to non-coaxial rotation of a porous disk and a fluid at infinity. Meccanica 2009;45(1):23–32. doi: https://doi.org/10.1007/s11012-009-9218-v.
[52] Ghara N, Guria M, Jana RN. Hall effects on oscillating flow due to eccentrically rotating porous disk and a fluid at infinity. Meccanica 2011;47(3):557–71. doi: https://doi.org/10.1007/s11012-011-9468-3.
[53] Mohamad AQ, Khan I, Ismail Z, Shafie S. Exact solutions for unsteady free convection flow over an oscillating plate due to non-coaxial rotation. Springerplus 2016;5(1):2090. doi: https://doi.org/10.1186/s40064-016-3748-2.
[54] Ersoy HV. Unsteady flow due to a disk executing non-torsional oscillation and a Newtonian fluid at infinity rotating about non-coaxial axes. Sādhanā 2017;42(3):307–15. doi: https://doi.org/10.1007/s12046-017-0600-5.
[55] Mohamad AQ, Khan I, Shafie S, Isa ZM, Ismail Z. Non-coaxial rotating flow of viscous fluid with heat and mass transfer. Neural Comput Appl 2017;30 (9):2759–69. doi: https://doi.org/10.1007/s00521-017-2854-6.
[56] Mohamad AQ, Khan I, Jiann LY, Shafie S, Isa ZM, Ismail Z. Double convection of unsteady MHD non-coaxial rotation viscous fluid in a porous medium. Bull Malays Math Sci Soc 2018;41(4):2117–39. doi: https://doi.org/10.1007/s40840-018-0627-8.
[57] Mohamad AQ, Khan I, Shafie S. Magnetic effects on second grade fluid flow due to non coaxial rotation of a disk through a porous medium with double diffusion. J Magn 2019;24(3):379–91. doi: https://doi.org/10.4283/JMAG.2019.24.3.379.
[58] Mohamad AQ, Ismail Z, Omar NFM, Qasim M, Zakaria MN, Shafie S, et al. Exact solutions on mixed convection flow of accelerated non-coaxial rotation of MHD Viscous fluid with porosity effect. Deffect Diffus Forum 2020;399:26–37. doi: https://doi.org/10.4028/www.scientific.net/DDF.399.26.
[59] Tiwari RK, Das MK. Heat transfer augmentation in a two-sided lid-driven differentially heated square cavity utilizing nanofluids. Int J Heat Mass Trans 2007;50(9–10):2002–18. doi: https://doi.org/10.1016/j.ijheatmasstransfer.2006.09.034.
[60] Xue QZ. Model for thermal conductivity of carbon nanotube-based composites. Physica B Condens Matter 2005;368(1–4):302–7. doi: https://doi.org/10.1016/j.physb.2005.07.024.
[61] Villinger H. Solving cylindrical geothermal problems using Gaver-Stehfest inverse Laplace transform. Geophysics 1985;50(10):1581–7. doi: https://doi.org/10.1190/1.1441848.
[62] Stehfest H. Algorithm 368: numerical inversion of Laplace transforms [D5]. Commun ACM 1970;13(1):47–9. doi: https://doi.org/10.1190/1.1441848.

Wan Nura'in Nabilah Noranuar has obtained her B.Sc. in Mathematics on November 2019. She is currently a Master of Philosophy (Mathematics) student from Department of Mathematical Sciences, Faculty of Sciences, Universiti Teknologi Malaysia, 81310 Johor Bahru, Johor, Malaysia. Her interest of research is fluid mechanics and advanced transport phenomena. Miss Wan Nura'in Nabilah Noranuar is member of Malaysian Mathematical Sciences Society.

Ahmad Qushairi Mohamad is a Senior Lecturer from Department of Mathematical Sciences, Faculty of Science, Universiti Teknologi Malaysia, 81310 Johor Bahru, Johor, Malaysia. He received his B.Sc. (2012), M.Sc. (2014) in Mathematics, and Ph.D. (2018) in Applied Mathematics from Universiti Teknologi Malaysia. His research interests are fluid mechanics, heat transfer and advanced transport phenomena. Dr. Ahmad Qushairi Mohamad is member of Malaysian Mathematical Sciences Society.

Sharidan Shafie obtained his B.Sc. (1992) and M.Sc. (1996) in Mathematics, and Ph.D. (2005) in Applied Mathematics from Universiti Teknologi Malaysia. His major research interests are fluid mechanics and heat and mass transfer. Dr. Sharidan is working as an Associate Professor at Department of Mathematical Sciences, Faculty Sciences, UTM. He is member of Malaysian Mathematical Sciences Society. He has published a number of research papers in Journal and Conferences in professional societies.

Ilyas Khan received his M. Phil from Quaid-i-Azam University Islamabad, Pakistan, Ph.D. and Post Doc from Department of Mathematical Sciences, Faculty of Science, Universiti Teknologi Malaysia (UTM) Johor Bahru, Johor. His field of interest is analytical and numerical solutions of Newtonian and non-Newtonian fluids. Dr. Khan has several years of teaching and research experience and currently he is working as an Associate Professor at Department of Basic Sciences, College of Engineering Majmaah University, Saudi Arabia.

Lim Yeou Jiann obtained his B.Sc. (2011), M.Sc. in Mathematics (2013) and Ph.D. in Applied Mathematics (2017) from Universiti Teknologi Malaysia. His research interest is fluid mechanic, heat transfer, numerical solutions and advanced transport phenomena. Currently, he is working as the research assistant under Department of Mathematical Sciences, Faculty of Science, Universiti Teknologi Malaysia, 81310 Johor Bahru, Johor, Malaysia.

Mohd Rijal Ilias obtained his B.Sc., M.Sc in Engineering Mathematics, and Ph.D. in Mathematics from Universiti Teknologi Malaysia. His research interest is boundary layer flow of heat and mass transfer. Currently, he is working under Centre of Mathematics Studies, Faculty of Computer and Mathematical Sciences, Universiti Teknologi MARA (UiTM), 40450 Shah Alam, Selangor, Malaysia.